Prediction of Landfalling Hurricanes with the Advanced Hurricane WRF Model

CHRISTOPHER DAVIS,* WEI WANG,* SHUYI S. CHEN,+ YONGSHENG CHEN,* KRISTEN CORBOSIERO,#
MARK DEMARIA,@ JIMY DUDHIA,* GREG HOLLAND,* JOE KLEMP,* JOHN MICHALAKES,*
HEATHER REEVES,& RICHARD ROTUNNO,* CHRIS SNYDER,* AND QINGNONG XIAO*

* *National Center for Atmospheric Research,** Boulder, Colorado*
+ *Rosenstiel School of Marine and Atmospheric Science, University of Miami, Miami, Florida*
# *University of California, Los Angeles, Los Angeles, California*
@ *NOAA/NESDIS, Fort Collins, Colorado*
& *National Severe Storms Laboratory, Norman, Oklahoma*

(Manuscript received 9 November 2006, in final form 24 August 2007)

ABSTRACT

Real-time forecasts of five landfalling Atlantic hurricanes during 2005 using the Advanced Research Weather Research and Forecasting (WRF) (ARW) Model at grid spacings of 12 and 4 km revealed performance generally competitive with, and occasionally superior to, other operational forecasts for storm position and intensity. Recurring errors include 1) excessive intensification prior to landfall, 2) insufficient momentum exchange with the surface, and 3) inability to capture rapid intensification when observed. To address these errors several augmentations of the basic community model have been designed and tested as part of what is termed the Advanced Hurricane WRF (AHW) model. Based on sensitivity simulations of Katrina, the inner-core structure, particularly the size of the eye, was found to be sensitive to model resolution and surface momentum exchange. The forecast of rapid intensification and the structure of convective bands in Katrina were not significantly improved until the grid spacing approached 1 km. Coupling the atmospheric model to a columnar, mixed layer ocean model eliminated much of the erroneous intensification of Katrina prior to landfall noted in the real-time forecast.

1. Introduction

As noted by Elsberry (2005), the prediction of hurricane track has advanced to the point where the original goals of the U.S. Weather Research Program (USWRP) have been achieved. That is not to say that the track problem has been solved, but rather that the community has been on a clear path toward improvement for many years. The use of coarse-grid prediction models, especially global models, has proved increasingly successful (Goerss 2006), which indicates that high resolution is not a requirement for improved track prediction.

The situation with intensity prediction is far more complicated, and progress has been generally slower. The primary reason for the slower progress was stated in Marks and Shay (1998): track prediction depends more on large-scale processes, and intensity depends on the inner-core dynamics and its relationship to the environment. That is, intensity is a multiscale problem. Only recently has the computational capability to address multiple scales of convection (cell scale, mesoscale, and synoptic scale) been achieved. The requirement to resolve the inner core, including the eyewall, the eye, and inner spiral rainbands near the eyewall, has led to the application of models with grid lengths of only a few kilometers (e.g., Liu et al. 1997; Zhu et al. 2004; Yau et al. 2004; Wong and Chan 2004; Krishnamurti 2005; Braun et al. 2006; Chen 2006).

At grid lengths of roughly 4 km or less, it has been shown that simulations with explicit treatment of continental, organized convection exhibit more realistic structure and movement than simulations relying on parameterized convection (Fowle and Roebber 2003; Done et al. 2004). However, the convection in a hurricane is strongly constrained by the secondary circulation. Furthermore, updrafts in tropical cyclones tend to

** The National Center for Atmospheric Research is sponsored by the National Science Foundation.

Corresponding author address: Christopher A. Davis, P.O. Box 3000, Boulder, CO 80307.
E-mail: cdavis@ucar.edu

DOI: 10.1175/2007MWR2085.1

be smaller and weaker than in midlatitude convection. Therefore, it is unclear whether the distinction between explicit and parameterized treatment of convection in tropical cyclones can be inferred from simulations of midlatitude convection. The related practical question is whether a mesoscale model with a grid spacing fine enough to forego cumulus parameterization actually offers improved prediction of the track, intensity, and structure of hurricanes. Beyond the resolution dependence, other key issues for hurricane prediction include the effect of mixing-induced ocean-surface cooling, treatment of fluxes at the air–sea interface, and improvement of the initial vortex structure through data assimilation. These issues are each made more prominent by the push toward finer spatial resolution in models.

The present paper represents an evaluation of the skill of explicit forecasts of tropical cyclones using the Advanced Research Weather Research and Forecasting (WRF) Model (ARW; Skamarock et al. 2005). So far, the performance of explicit hurricane simulations has been evaluated only for case studies, not in a statistical sense. By examining multiple forecasts from five landfalling hurricanes in a real-time setting, the potential of the ARW for predicting hurricane intensity and structure will be assessed. The operational realization of fully explicit hurricane forecasts may still be a few years away, but computational capabilities have increased to the point that such forecasts can be run in real time, thereby facilitating examination of many cases. Therefore, this work offers a glimpse into the next generation of hurricane forecasts.

The present paper is divided into two general themes. First, the performance of the ARW core for real-time prediction efforts during the 2005 hurricane season (sections 2 and 3) is summarized. The second part of the paper constitutes a case study of Katrina, with a limited suite of sensitivity analyses addressing many of the shortcomings evident in real-time forecasts. The representation of air–sea fluxes (section 4), storm-induced upper-ocean cooling (section 5), and model resolution (section 6) are investigated as key areas for improving forecasts. Other physical processes within the atmospheric model clearly affect tropical cyclone (TC) intensity, such as cloud physics and the boundary layer parameterizations, but these are not considered explicitly herein. Similarly, the topic of model initialization, an important component of short-range prediction, will be considered in a future article. The outcome of analyzing the effect of model permutations will provide guidance for improved configurations of future real-time and research simulations.

2. Model configuration

The real-time ARW forecasts in 2005 used a two-way nested configuration (Michalakes et al. 2005), that featured a 12-km outer fixed domain with a movable nest of 4-km grid spacing. The nest was centered on the location of the minimum 500-hPa geopotential height within a prescribed search radius from the previous position of the vortex center (or within a radius of the first guess, when first starting). Nest repositioning was calculated every 15 simulation minutes and the width of the search radius was based on the maximum distance the vortex could move at 40 m s^{-1}. In later sections of the paper, simulations with a further mesh refinement to 1.33-km grid spacing will be discussed. In these simulations, the 1.33-km nest determined the location of the 4-km nest such that both were centered on the hurricane.

On the 12-km domain, the Kain–Fritsch cumulus parameterization was used, but domains with finer resolution had no parameterization. All domains used the WRF single-moment 3-class (WSM3) microphysics scheme (Hong et al. 2004) that predicted only one cloud variable (water for $T > 0$°C and ice for $T < 0$°C) and one hydrometeor variable, either rainwater or snow (again thresholded on 0°C). Both domains also used the Yonsei University (YSU) scheme for the planetary boundary layer (Noh et al. 2003). This is a first-order closure scheme that is similar in concept to the scheme of Hong and Pan (1996), but appears less biased toward excessive vertical mixing as reported by Braun and Tao (2000). The drag formulation follows Charnock (1955) and is described more in section 5. The surface exchange coefficient for water vapor follows Carlson and Boland (1978), and the heat flux uses a similarity relationship (Skamarock et al. 2005).

The forecasts were integrated from 0000 UTC and occasionally 1200 UTC during the time when a hurricane threatened landfall within 72 h. Forecasts were initialized using the Geophysical Fluid Dynamics Laboratory (GFDL) model, with data on a ⅙° latitude–longitude grid. The Global Forecast Model (GFS) from the National Centers for Environmental Prediction (NCEP), obtained on a 1° grid, was used only when the GFDL was unavailable. Experimental forecasts were integrated during the 2004 hurricane season using a GFS initial condition, and the results were generally found to be inferior to results from forecasts initialized with the GFDL. This is not surprising because of the more sophisticated bogusing scheme used in the GFDL model (Bender 2005), and the sixfold decrease of the grid spacing in the GFDL analysis relative to the archived GFS fields.

Several systematic errors in ARW were found during examination of the real-time forecasts after the season. The most severe of these resulted from an underestimate of the surface momentum exchange over water due to a coding error. The reduced drag led to a larger radius of maximum wind, presumably because near-surface parcels were unable to flow across angular momentum surfaces. This coding error, along with other, minor errors, has been corrected in the most recent version of the ARW, release 2.1.2 (January 2006). This release is the baseline for extensions of ARW specifically intended for hurricane prediction. The ARW thus augmented for hurricane forecasts is termed the Advanced Hurricane WRF (AHW). In what follows, we will also use the acronym AHW to refer to real-time forecasts conducted during 2005, even though the model at that time was not modified specifically for hurricane prediction. The AHW is distinct from the Hurricane WRF (HWRF) run by NCEP that is based on the Nonhydrostatic Mesoscale Model (NMM; Janjic 2004).

3. Statistics for 2005

The forecasts from the 2005 season were evaluated using the traditional metrics of hurricane position error and intensity error. Intensity is assessed using the maximum sustained wind at 10-m elevation. Whereas observations are based on a 1-min average, the model output is instantaneous. However, the time step on the 4-km grid is 20 s. The fact that several time steps are needed to resolve temporal variations means that, at this resolution, instantaneous output should be roughly comparable to a 1-min average.

Intensity and position forecasts from the AHW were verified against the best-track data from the National Oceanic and Atmospheric Administration (NOAA) National Hurricane Center (NHC) and were compared with several other forecast techniques for the same periods during the 2005 season (Fig. 1). The sample shown in Fig. 1 is homogeneous (i.e., all forecast techniques were initialized and validated at the same times as the AHW). Sample size decreased from 34 at short time ranges to 19 at 72 h. As the forecast progressed, the relative skill of the 4-km forecasts increased for both position and intensity. Beyond 24 h, the position errors were smaller than either the official forecast or from the GFDL model. By 72 h, the intensity forecast errors were smaller than for the other techniques shown in Fig. 1. By this time, the intensity bias in AHW4 was $+4.5\ \mathrm{m\ s^{-1}}$ (not shown). For all other forecast intervals, intensity biases were smaller than $2\ \mathrm{m\ s^{-1}}$. Unique to the AHW, there was no monotonic growth of intensity

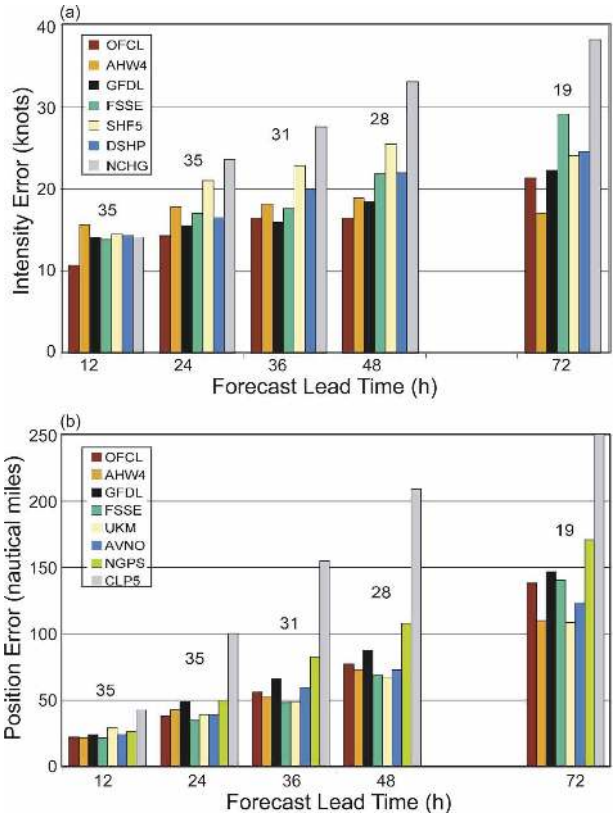

FIG. 1. Intensity (kt) and position (n mi) errors for the AHW forecasts run with an inner moving nest of 4-km grid spacing during 2005. Results from other forecast techniques are defined as Official (OFCL), AHW 4 km (AHW4), GFDL hurricane Model (GFDL), Florida State University Super Ensemble (FSSE), the statistical 5-day National Hurricane Center statistical model (SHIFOR) model (SHF5) and Decay SHIP (DSHP) techniques, the Met Office (UKMO), the NCEP Aviation Model (AVNO), the Navy Operational Global Atmospheric Prediction System (NOGAPS) model (NGPS), the statistical climatology and persistence (CLIPER) model (CLP5), and no change (NCHG). Sample sizes appear above each set of color bars.

error with time. The slower growth of wind speed errors compared to position errors is partly due to the fact that the winds are relative to the storm and are therefore position corrected. While statistical significance is difficult to demonstrate with the modest sample sizes reported herein, the main point to be drawn from the results is that the AHW is highly competitive with, and sometimes superior to, operational forecasts of position and intensity beyond about one day.

Time series of observed and predicted maximum wind for Katrina, Ophelia, Rita, and Wilma (Fig. 2) show that the real-time forecasts had difficulty capturing situations during which rapid intensification occurred, especially if it happened soon after initialization (Figs. 2a,c,d). Many forecasts featured spikes in maxi-

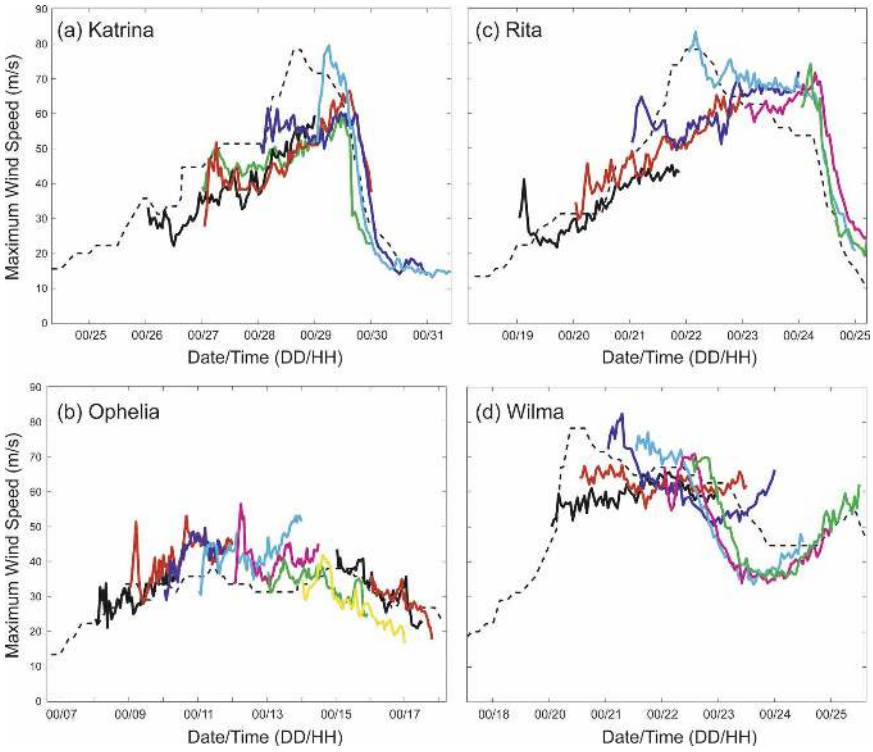

FIG. 2. Maximum sustained wind from best-track data (dashed) and from 25 forecasts covering four storms using the moving nest of 4-km grid spacing. Colors are used to distinguish forecasts but have no specific meaning; (a) Katrina; (b) Ophelia; (c) Rita; and (d) Wilma. The green curve in (a) denotes the two-domain retrospective simulation of Katrina initialized with the GFDL data.

mum wind speed within 6–12 h of initialization. These spikes indicate significant adjustment of the AHW to the initial state as prescribed by the GFDL-model-based analysis. The structure of the initial vortex in the GFDL model depends heavily on the physics of that model (Bender 2005). It is perhaps not surprising that, when inserted into a model with different numerical schemes and physical parameterizations such as AHW, an inconsistency can result. The adjustment early in the AHW forecast likely contributed to its relatively poor intensity forecast in the first 24 h (Fig. 1).

Forecasts for Katrina and Rita intensified the hurricane until landfall, whereas the real storms weakened notably from their maximum intensity prior to landfall (Figs. 2a,c). The rate of weakening following landfall appeared well predicted. Forecasts for Ophelia, a storm with more modest intensity changes, exhibited relatively smaller errors than other forecasts (Fig. 2b).

Examples of near-surface wind-field forecasts for four storms (Fig. 3) indicate that many structural aspects were well predicted, but some systematic errors existed. For observed winds, the HWind product from the Hurricane Research Division of the Atmospheric, Oceanic, and Marine Laboratory of NOAA was used. To facilitate comparison of forecast and analyzed winds, the position of the model storm center was shifted to the observed location. The variation of the radius of hurricane-force winds (33 m s^{-1}) among the cases was generally well forecast. The erroneously large core of Katrina resulted from initializing with the GFS analysis for this particular real-time forecast, coupled with the deficiency in the surface drag noted previously. The relatively small extent of Ophelia's circulation was well predicted, as were the major asymmetries in Katrina and Wilma. Some errors in storm structure were due to position errors relative to the coastline, thereby placing the wrong portion of the wind field over land where there was greater surface friction. The forecast of Rita shown (Fig. 3c) had the largest error of any forecast in the 2005 sample.

A comparison of observed and simulated radar reflectivity patterns using the WSI Corporation "NOWrad" reflectivity product and the column maximum reflectivity computed from the AHW hydrometeor fields

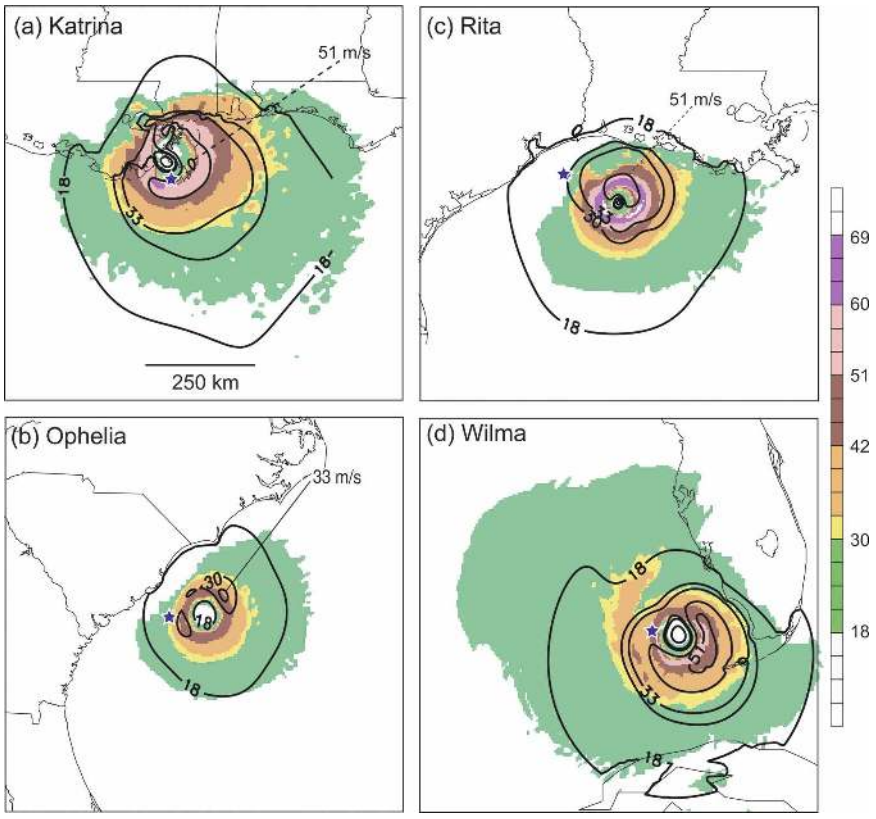

FIG. 3. Shown here is 10-m wind from AHW real-time forecasts performed during 2005, with contours of HWind analyses overlaid. Predicted storm center location at indicated valid times (below) is denoted by blue star in each figure. Wind fields from AHW forecasts have been shifted to observed locations to facilitate comparison. Model valid times are (a) Katrina, valid time = 1200 UTC 29 Aug (60-h forecast); (b) Ophelia, valid time = 0000 UTC 14 Sep (72-h forecast); (c) Rita, valid time = 0000 UTC 23 Sep (72-h forecast); and (d) Wilma, valid time = 0900 UTC 24 Oct (69-h forecast). HWind valid times are (a) 1132 UTC 29 Aug, (b) 0130 UTC 14 Sep, (c) 2303 UTC 23 Sep, and (d) 0730 UTC 24 Sep.

(rain and snow)[1] shows that the model was able to discriminate several major precipitation features (Fig. 4). The major asymmetries in the rainfall were generally well predicted, including the large rain shields in the outer rainbands to the northwest of Katrina and Rita, and to the north and northeast of Wilma associated with a surface frontal boundary (not shown). Katrina and Rita each had multiple, cellular convective bands to the east of the center and these appear in the model. Wilma featured deep convection cells to the northeast of the center over Florida. In addition, the size of the rain shield was predicted well in each case, with Ophelia being clearly smaller than the other cases.

Perhaps the most obvious deficiency in forecast precipitation structure was the high bias in simulated reflectivity. Offshore, attenuation of the radar beam coupled with the elevation of the lowest scan angle of the Weather Surveillance Radar-1988 Doppler (WSR-88D; 0.5°) means that the radar may underestimate reflectivity. However, the bias is still evident over land, which implies deficiencies in the model microphysical scheme. Although detailed precipitation verification has not been performed for these cases, the ARW on a 4-km grid has been noted to have a positive bias for rainfall (Done et al. 2004). Another deficiency is that convection tended to appear as larger cells rather than continuous bands on the 4-km grid.

The time dependence of the recurring types of intensity errors can be summarized by examining time series of forecasts of Hurricane Katrina (Fig. 5). The maximum 10-m wind of 26 m s^{-1} from the real-time forecast was initially smaller than the best-track value of 46

[1] See Koch et al. (2005) for an overview of using reflectivity fields for evaluating numerical simulations.

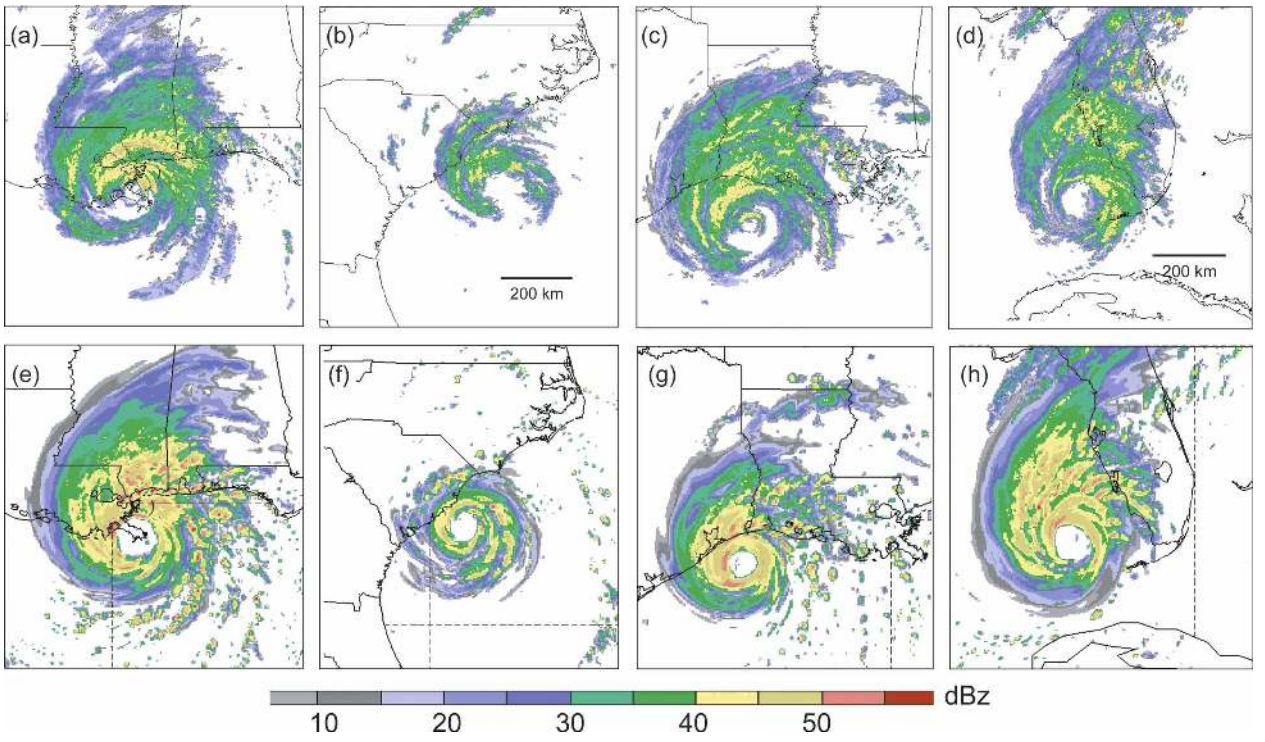

FIG. 4. Composite reflectivity from the (a)–(d) WSI Corporation NOWrad product and (e)–(h) AHW real-time forecasts. Valid times are as in Fig. 3; (a) and (e) are valid at 1200 UTC 29 Aug (Katrina), (b) and (f) are valid at 0000 UTC 14 Sep (Ophelia), (c) and (g) are valid at 0000 UTC 24 Sep (Rita), (d) is valid at 0730 UTC 24 Oct, and (h) is valid at 0900 UTC 24 Oct.

m s^{-1}. This discrepancy was due primarily to the use of the 1° latitude–longitude NCEP GFS analysis for initialization in this particular forecast. The GFDL forecast was not available in real time for this particular case but was obtained for retrospective simulations (see below). Within the first hour of integration, the storm intensity from the real-time forecast rapidly increased to nearly the observed intensity, only to decrease and remain well below the observed intensity for the next 48 h (Fig. 5a).

The minimum sea level pressure in the real-time forecast of Katrina was much greater than observed (Fig. 5b), even when the maximum winds were comparable. This is hypothesized to be occur because the surface friction was too weak, which resulted in a large, nearly stagnant eye as air parcels were relatively unable to flow across angular momentum surfaces into the inner core. This obvious problem was corrected with any reasonable choice of surface drag formulations (section 4), although the timing of the sea level pressure changes for Katrina was still incorrect and broadly consistent with timing errors in maximum wind speed.

Recent results by Chen (2006) and Chen et al. (2007) have suggested that proper treatment of the inner core requires a grid spacing less than 2 km. To investigate the resolution dependence of intensity forecasts in the case of Katrina, forecasts were rerun using the single-domain 12-km grid and separately the two-domain configuration with a moving nest on a 4-km grid. In another simulation, a second moving nest with 1.33-km grid spacing was added, centered within the 4-km grid. The 4-km domain used in the three-domain simulation (202 × 202 points) was smaller than that used for the real-time forecasts (316 × 310 points). The 1.33-km grid contained 241 points on a side, and covered an area of 320 km × 320 km. The three-domain simulations required about 2.6 times more computing time than the real-time forecasts, using the same processor configuration [128 processors on the Bluesky (IBM-SP) at the National Center for Atmospheric Research]. The retrospective simulations all used the most recent version of ARW (version 2.1.2) wherein the error in surface drag over the ocean had been corrected. These simulations were also begun with the initial state from the GFDL model.

The initial intensity error was tempered by the use of the GFDL data, and this error reduction was evident through at least 12 h, although the improvement was not dramatic. The observed period of rapid intensification of Katrina was not captured in the real-time fore-

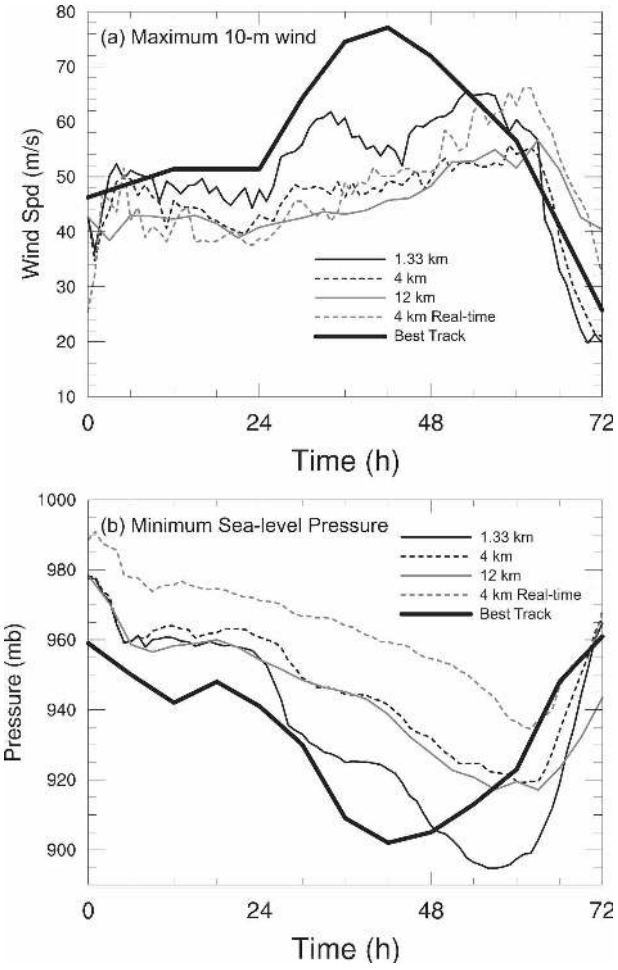

FIG. 5. (a) Maximum 10-m wind and (b) minimum sea level pressure for forecasts of Katrina beginning 0000 UTC 27 Aug. Legend labels 1.33, 4, and 12 km refer to grid spacing of WRF ARW, version 2.1.2, using the Charnock drag relation. The forecast on a 12-km grid used the Kain–Fritsch parameterization. The 4-km real time (gray dashed) refers to the forecast made in real time with an innermost nest of 4-km grid spacing. All retrospective forecasts were initialized with the GFDL initial condition.

casts, nor was it captured in the updated AHW with GFDL initial conditions and a finest grid spacing of 4 km or coarser. Only with the second nest of 1.33-km grid spacing was there a signature of rapid intensification early on 28 August, consistent with the results of Chen (2006). All forecasts produced peak intensity just prior to landfall. Recall that a qualitatively similar error occurred in other forecasts of Katrina and for Rita as well (Fig. 2). The major contributors to this error appeared to be both the neglect of the feedback of ocean mixing on sea surface temperature (SST), and possibly the use of an unreasonably high SST. The SSTs near the Gulf Coast exceeded 31°C in the Reynolds SST analysis used as the temporally fixed lower boundary condition. Even if such high SSTs existed prior to storm passage, they were likely not present beneath the eyewall (Scharroo et al. 2005; section 5 herein).

Given the noted errors for the 2005 real-time forecast experiments, and the behavior of the real-time and retrospective simulations of Katrina (Fig. 5), three general areas crucial for forecast error reduction were identified: 1) improved surface-entropy-flux formulation, 2) incorporation of the effects of storm-induced ocean mixing on SST, and 3) finer resolution in the inner core. In the following three sections, the effect of modeling advances in each of these three areas on position and intensity forecasts of Katrina is examined. Improved initialization of the storm structure and intensity was also identified as a crucial element of improved forecasts, but a proper treatment of this topic is too lengthy to be presented here and the optimal initialization strategy for AHW is not yet known.

4. Surface-flux formulation

Past studies (e.g., Emanuel 1995; Braun and Tao 2000; Bao et al. 2002; Chen et al. 2007) have shown that simulated hurricane intensity is quite sensitive to the surface-flux parameterizations of both momentum and enthalpy (heat and moisture). Herein the sensitivity of the AHW forecasts of Katrina to such parameterizations is explored.

The surface stress parameterization in the control simulation uses a Charnock (1955) relation between the roughness length z_0 and frictional velocity u_*, given as $z_0 = c_{z_0}(u_*^2/g) + o_{z_0}$, where $c_{z_0} = 0.0185$ and $o_{z_0} = 1.59 \times 10^{-5}$ m. Note that this relation is recursive because the friction velocity depends on roughness length and vice versa, but in practice the model formulations use values from the previous time step and achieve convergence quickly. The drag coefficient can be defined as $C_D = (u_*^2/V^2)$, where V is the wind speed at a reference height (10 m). In terms of the 10-m drag coefficient, the Charnock relation gives a drag coefficient that generally increases from about 0.001 to 0.003 at hurricane wind strengths, and it would increase to 0.005 for wind speeds associated with category 5 storms (>70 m s^{-1}). However, observational evidence (e.g., Black et al. 2007) suggests that it remains near 0.003 for high wind speeds.

An alternate drag formulation based on the high-wind wind-tunnel studies of Donelan et al. (2004) was also investigated. These results produced values of C_d lower than those from the Charnock relation for low winds with a linear increase up to a maximum near 0.0024 at about 35 m s^{-1}. Fitting this proportional behavior between C_d and V at 10 m gives a relation $z_0 =$

$10 \exp(-10/u_*^{1/3})$, with a lower and upper limit on z_0 of 0.125×10^{-6} and 2.85×10^{-3} m, respectively.

The differences in the two drag formulations for simulations of Katrina are exhibited in Fig. 6. The Donelan formulation, with less drag than the Charnock formulation, results in higher wind speeds but also higher central pressures and a slightly larger eyewall radius. Each of these changes in storm characteristics represents an improvement in the simulation of Katrina. The relationship between drag, pressure perturbation, and eyewall radius agrees qualitatively with that reported in section 3, although here the difference in drag between the two drag formulations is relatively smaller. It must be pointed out that the real drag force on surface winds is determined by the time-evolving ocean wave spectrum, prediction of which requires a wave model (e.g., Chen et al. 2007). Therefore the drag parameterizations discussed above must be considered as crude representations of the bulk effects of waves in hurricanes.

The surface heat and moisture fluxes require, in addition to the friction velocity discussed above, a scaling temperature θ_* or moisture q_* that defines the similarity theory profile (a log profile in neutral conditions). This parameter can be regarded as representing how easily surface heat- or moisture-transporting eddies grow from molecular to vertically resolved scales in the surface layer of the atmosphere. Standard treatments of the effect of stability by Paulson (1970) and Webb (1970) differ in the effect of wind speed on this part of the flux, especially over water. Several schemes use a friction-velocity Reynolds number to define a molecular viscosity sublayer roughness length z_{0h}, $\mathrm{Re}_* = (u_* z_{0h}/\nu)$, where ν is the molecular viscosity of air. This leads to an inverse relationship between roughness length and wind speed, and has the effect of a resistance to the eddy scalar transports that increases with wind speed. Therefore the q_* contribution to the surface moisture flux $u_* q_*$ tends to oppose the effect of u_* increasing with wind speed (similarly for heat and enthalpy). The transfer coefficient C_q is defined from $C_q = (u_* q_*/V\Delta q)$, where V and Δq are the wind speed and difference in water vapor mixing ratio between the surface and reference level (taken conventionally at 10 m). A similar coefficient C_θ can be defined for heat using potential temperature θ_*. The coefficient C_k is defined for the exchange of enthalpy using the combination $c_p\theta_* + L_v q_*$.

Because of the various parameterizations of wind speed effects in q_* or θ_*, C_k can increase slowly with wind speed (Carlson and Boland 1978), stay steady with wind speed (Large and Pond 1981), or decrease with wind speed (Garratt 1992). In the Carlson–Boland formulation used for retrospective simulations, it is assumed that $C_k = C_\theta = C_q$ rather than using similarity theory for the heat flux as was done in the real-time forecasts. With the Donelan drag formulation, the effect of using constant $C_k = 0.001$ (as in the Large and Pond formulation) is to reduce the maximum wind during the period 24–48 h by roughly 15% compared to the result using the Carlson–Boland scheme, that has a C_k value of about 0.0015 (Fig. 7). This sensitivity is slightly less than would be inferred from the dependence of maximum wind on $(C_k/C_d)^{1/2}$, derived by Emanuel (1995), wherein a wind speed reduction of 22% would be obtained. While the proper wind speed dependence of C_k remains a topic of active research (Black et al. 2007), the point of the above calculations is to demonstrate that the sensitivity of the AHW to the particular

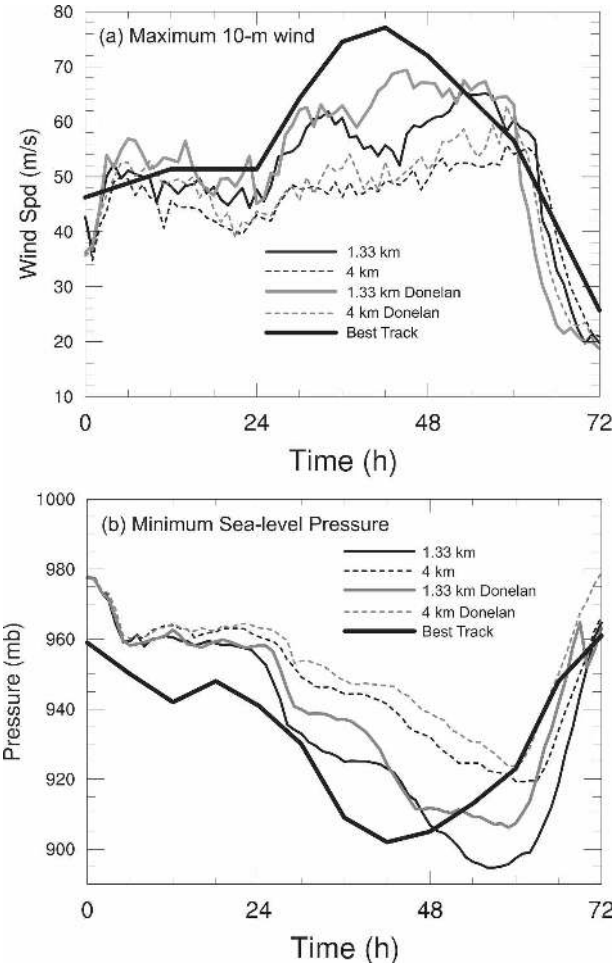

FIG. 6. (a) Maximum 10-m wind and (b) minimum sea level pressure for forecasts of Katrina beginning 0000 UTC 27 Aug. Data from forecasts using a 1.33-km (4 km) innermost grid appear as solid (dashed) lines; gray for the forecast using the Donelan drag formulation.

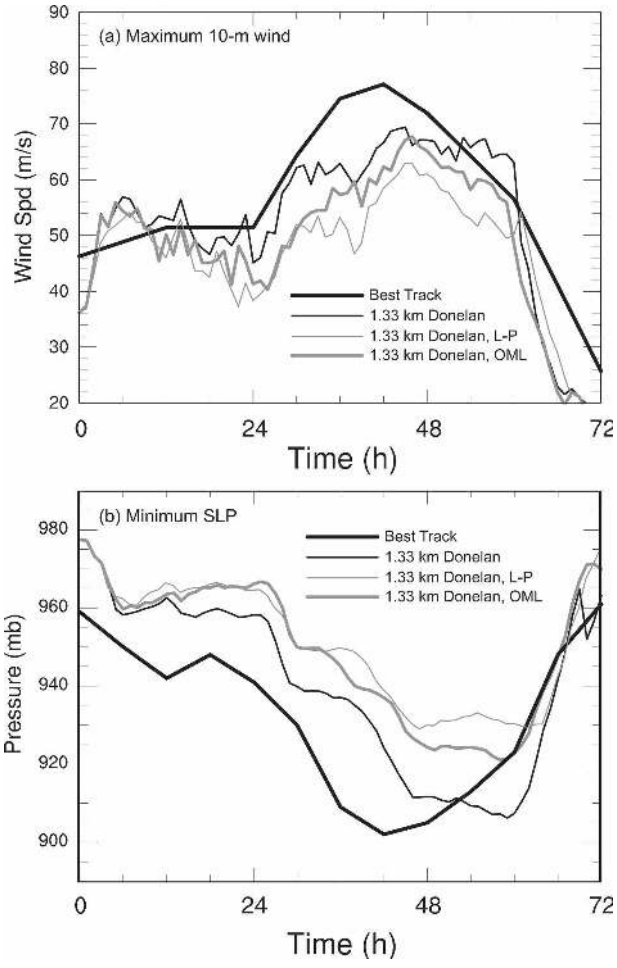

FIG. 7. (a) Maximum 10-m wind and (b) minimum sea level pressure for forecasts of Katrina beginning 0000 UTC 27 Aug. All time series taken from simulations with innermost grid spacing of 1.33 km initialized with GFDL. Heavy black line denotes best-track data; thin black line denotes the Donelan experiment (from Fig. 6); thin gray line denotes simulation using the Large and Pond [constant (C_k)] enthalpy exchange coefficient; thick gray line denotes the simulation with the ocean mixed layer (section 5) and Carlson–Boland enthalpy flux.

formulation agrees reasonably well with theoretical estimates.

5. Ocean feedback

To forecast the ocean temperature feedback in the AHW hurricane forecasts a simple mixed layer ocean model has been applied in individual columns at every grid point. The mixed layer ocean model is used in the spirit of a parameterization rather than a realistic treatment of an evolving ocean in the presence of a hurricane vortex. In view of the errors of the short-range intensity forecasts (section 3), and recent work by Emanuel et al. (2004), it is argued herein that the first-order negative feedback of wind-driven ocean mixing on hurricane intensity can be captured by a simple and computationally inexpensive model.

The mixed layer model follows that of Pollard et al. (1973), except that our implementation allows for nonzero initial mixed layer depth. The model is based on the assumption of no heat transfer between the individual columns so that temperature changes within a column can occur only through vertical redistribution. The wind field of the hurricane applies a stress to the top of an assumed turbulent mixed layer. The mixed layer deepens and cools it through entrainment of colder water from below. Whereas pressure gradients and horizontal advection are neglected, the Coriolis force is included. Therefore, local accelerations are forced by the stress, and currents undergo inertial rotation. Near-inertial motions dominate the mixed layer current response to hurricane passage on the time scale of order one day (Price 1981). Except for the inclusion of the Coriolis force, the mixed layer model is identical to that used by Emanuel et al. (2004) to study the oceanic feedback on an axisymmetric hurricane vortex.

The mixed layer ocean model requires specification of the surface stress at the top, an initial mixed layer depth h_0, and a deep-layer lapse rate Γ. The model can be operated as a single column, or an array of columns with a spatially varying h_0, Γ, and time-dependent stress driving each column. In reality, these parameters vary spatially, and their variation is crucial for representing the thermal influence of features such as the Loop Current in the Gulf of Mexico, the Gulf Stream, or warm and cold eddies. The initial current in the mixed layer is taken to be zero on the assumption that hurricane-induced currents are much greater than preexisting ones.

As a test of the model performance the results of Price (1981) have been reproduced in which a prescribed vortex translated over a multilevel, stratified ocean model with an initial temperature profile having a well-defined mixed layer depth of 30 m and a deep-layer lapse rate of 0.05 K m^{-1}. In both models, the maximum cooling was 3.1 K and cooling occurred almost entirely to the right of the storm track. It should be noted that, without a Coriolis force in the ocean model, the only source of cross-track asymmetry is in the wind stress itself. This factor alone is generally insufficient to explain the cross-track variation of ocean-surface cooling. Much of the observed cross-track asymmetry is believed to result from an inertial current that is systematically reinforced by the stress arising from the local veering of surface wind with time to the right of the track and cancelled because of the wind

backing to the left of the track (Price 1981). An enhanced current will increase mixing across the lower interface of the mixed layer. Greater mixing will reduce the sea surface temperature more for a given mixed layer depth.

The dynamic forcing for the mixed layer model as implemented in AHW is the friction velocity from the atmospheric model's surface layer physics. The ocean mixed layer model is called at every atmospheric model grid point and uses the same time step. The updated sea surface temperature is fed back to the atmospheric surface conditions.

To compute the mixing-induced cooling in the AHW, and its effect on storm intensity, the model was initialized at 0000 UTC 27 August as in section 4 using the GFDL initial condition and version 2.1.2 of ARW for the atmosphere. The initial mixed layer depth was set to 30 m everywhere, with Γ chosen to be 0.14 K m^{-1}. As expected, the swath of cooling was confined to the right of the storm track, with a maximum cooling of about 3.5°C (Fig. 8a). The net effect of the ocean cooling on the maximum surface winds was a reduction of roughly 8 m s^{-1} prior to landfall (Fig. 7).

While the predicted SST change beneath the eyewall is the key parameter influencing hurricane intensity, it cannot be verified directly in most cases. In practice, observations of the SST change are only available by comparing satellite observations prior and following the storm passage. The simulated and observed SST reduction maximized to the right of the storm track (Fig. 8b), but observed cooling was more spatially extensive. Furthermore, the observed cooling varied more along the axis of maximum temperature change parallel to the track, with SST changes ranging from about 2°–4.5°C. This variation may be due to several factors, but most prominent is the spatially varying upper-ocean thermodynamic structure.

Prior to the passage of Katrina, altimetry data showed the sea surface raised locally by approximately 20 cm along the hurricane's track (Scharroo et al. 2005) in association with the Loop Current and a warm-core ring farther to the northwest ("W" in Fig. 8b). Positive sea surface height is indicative of deep, warm water in the upper ocean and large heat content. For the same SST prior to the arrival of a storm, wind-driven mixing during storm passage would produce a smaller decrease in SST over a layer of high heat content than over a layer with low heat content. The mixed layer model can represent this effect on SST, and can accommodate arbitrary spatial variation of either the mixed layer depth or the deep-layer lapse rate because each column in the model integrates independently. An important research topic is how to use altimetry measurements and relatively rare thermodynamic profiles of the upper ocean to specify initial, spatially varying fields of mixed layer depth and deep-layer lapse rate in the mixed layer ocean model.

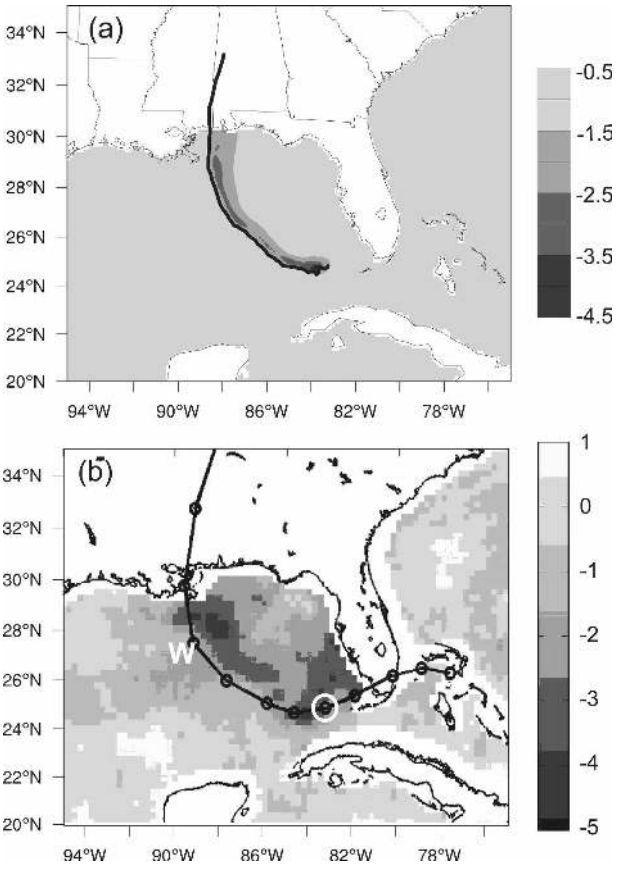

FIG. 8. (a) Change in SST (°C) produced during a 72-h three-domain simulation using AHW (same configuration as for 1.33-km nest in Fig. 5) coupled to the mixed layer ocean model with h_0 = 30 m and Γ = 0.14 K m^{-1}. Storm track is also indicated: (b) SST (°C) difference (31 Aug minus 25 Aug) derived from daily composite Tropical Rainfall Measuring Mission–Advanced Microwave Scanning Radiometer (TRMM–AMSR) data and observed storm track (black line) with 12-hourly positions indicated with circles. "W" in (b) indicates center of warm-core eddy. White circle in (b) denotes storm location at 0000 UTC 27 Aug.

6. Structure

The resolution dependence of various structural features in simulations of mature hurricanes was investigated using the retrospective simulations of Katrina discussed in section 3. The simulations described first in this section used the Charnock drag formulation (see section 4). In this case the inner-core structure of the hurricane vortex was generally not well represented by AHW on a 12-km grid (Fig. 9a). The observed radius of

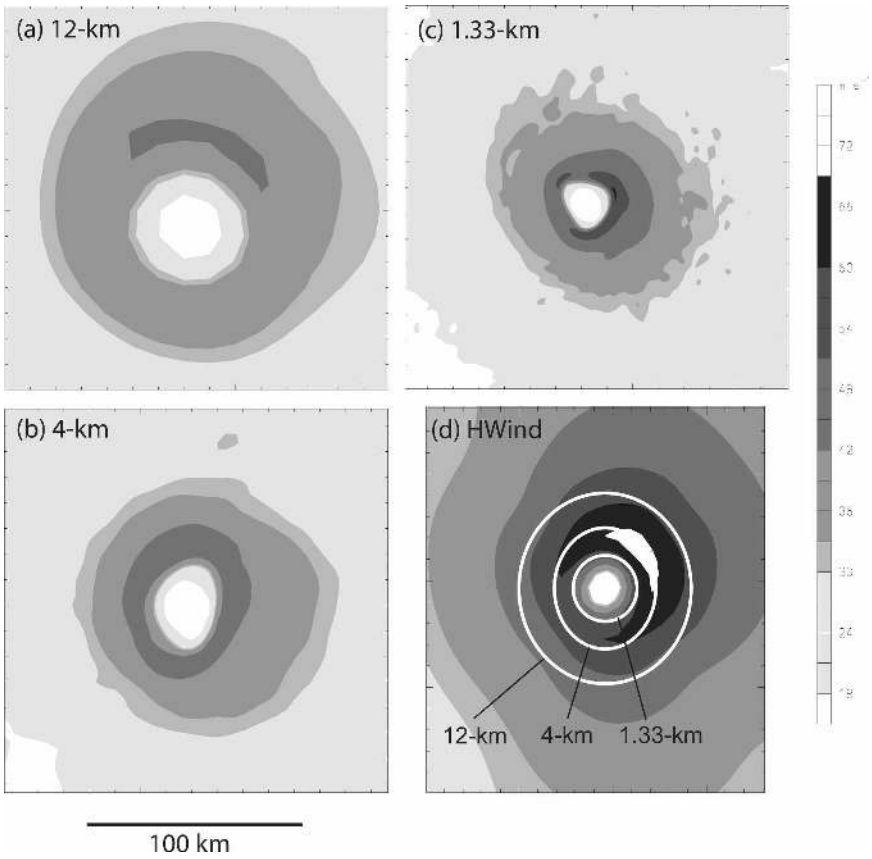

FIG. 9. Shown here is 10-m wind speed (m s^{-1}) from 36-h Katrina forecast valid 1200 UTC 28 Aug on (a) the 12-km grid, (b) the 4-km grid, (c) the 1.33-km grid, and (d) the NOAA HWind product valid 1200 UTC 28 Aug. White ellipses in (d) are an approximate trace of the radii of maximum wind at each azimuth around the vortices in (a), (b), and (c).

maximum wind in Katrina (Fig. 9d) was about 25 km at 1200 UTC 28 August. With potentially only four grid points across the eye, it is not surprising that the model integrated on 12-km grid had a radius of maximum wind of about 40 km. However, the extent of hurricane-force winds matched better the HWind analysis than either of the predicted wind fields in the 4- or 1.33-km simulations (Figs. 9b and 9c).

The finest-resolution forecast (Δx = 1.33 km) produced a radius of maximum wind of only 13 km (Fig. 9c), and contracted the hurricane-force winds far too much. The simulation with a 4-km innermost grid spacing (Fig. 9b) resulted in a radius of maximum wind close to that observed, although the maximum wind itself was less than observed and the extent of hurricane-force winds was too small. With the Donelan et al. (2004) drag law in the simulation using a 1.33-km grid (see Fig. 6), the radius of maximum wind expanded to about 18 km and the hurricane-force winds extended to about 60 km (not shown).

The overall result was that the predicted size of the circulation of Katrina, not just the radius of maximum wind, varied with the grid increment in the present case. The area covered by hurricane-force winds is of paramount importance in applications such as storm-surge forecasting. Here it is seen that this parameter depends on model resolution, even in the range of grid increments where the eye is theoretically well resolved. Considering results from sections 3 and 4 as well, it is hypothesized that storm size is influenced by the drag formulation (weaker drag results in a larger eye for a given storm) and model resolution.

Because of its improved vortex representation relative to the three-domain control simulation, the three-domain simulation using the Donelan drag formulation and Carlson–Boland flux formulations will be analyzed in the remainder of this section. To assess the vertical structure of winds in the eyewall, data were obtained from dropsondes deployed from the NOAA P-3 during the afternoon of 28 August (between about 1700 UTC 28 and 0000 UTC 29 August). Profiles at a radial distance of about 16 km on the 1.33-km AHW domain

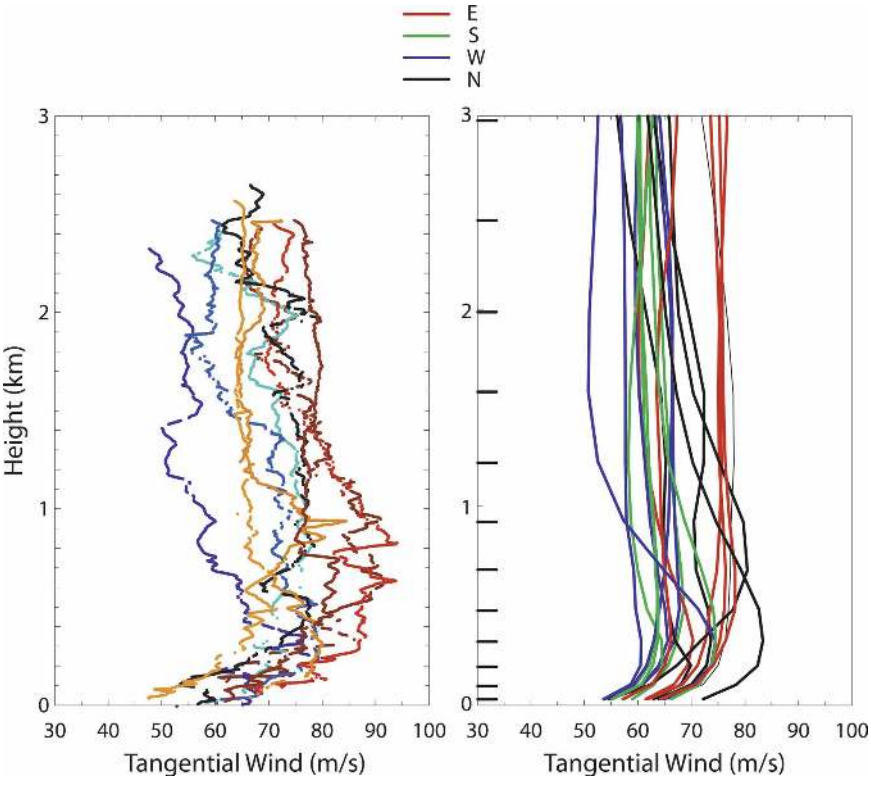

FIG. 10. Vertical profiles of tangential wind in the eyewall of Katrina between 1700 and 2300 UTC 28 Aug compared with actual dropsonde soundings. Colors indicate azimuthal location of the sounding as noted in key above (i.e., brown is northeast quadrant, orange is southeast, cyan is southwest, and violet is northwest). Heavy tick marks on ordinate in (b) indicate approximate altitude of model coordinate surfaces in the eyewall.

were taken during the period 1900–2300 UTC. The simulated profiles were selected in the eyewall along each of the four cardinal directions. Observed dropsondes were deployed in varying azimuthal locations within the eyewall (Fig. 10). Observed winds were converted to tangential and radial coordinates using center fixes determined at four times (1755, 1923, 2038, and 2325 UTC) by Hurricane Research Division flight scientists aboard a NOAA P-3. The center positions were linearly interpolated to the time of the dropsonde data.

Similarities between model and observed winds included the generally stronger winds in the east or northeast quadrant versus the southern or western sections, and the values of near-surface tangential winds (Fig. 10). The major differences were the lack of adequate vertical shear in most simulated profiles in the lowest 400 m and the absence of a simulated wind maximum near 700-m altitude in the northeast quadrant. The model predicted jets only 300 m above the surface in some instances, whereas only one observed profile has such a low-level wind maximum. Since there were only 11 model levels in the lowest 3 km, limited vertical resolution was perhaps one factor contributing to the reduced vertical wind shear in the AHW. Another factor was possibly excessive vertical mixing (Braun and Tao 2000).

Rainbands in simulations of Katrina appeared generally more realistic in the simulation with 1.33-km grid spacing than in the simulation on a 4-km grid (Fig. 11). A comparison of the simulated reflectivity with airborne Doppler radar reflectivity observations from the NOAA P-3 and Naval Research Laboratory P-3 aircraft (Fig. 11c) revealed increasing cellularity of precipitation features with distance from the storm center. The finer-resolution simulation had a primary rainband to the east of the center, whereas the observations indicate a similar structure at a greater radius, consistent with the greater extent of the observed hurricane wind field. From the more detailed perspective of Fig. 11 and the larger-scale perspective of Fig. 4, it appears that explicit convection in the outer rainbands on a 4-km grid is unrealistic on the scale of cells, although the cells may be aligned in bands that correspond qualitatively with observed outer rainbands.

Beyond 36 h into the Katrina simulation on the 1.33-km grid, the inner edge of the eyewall took on a range

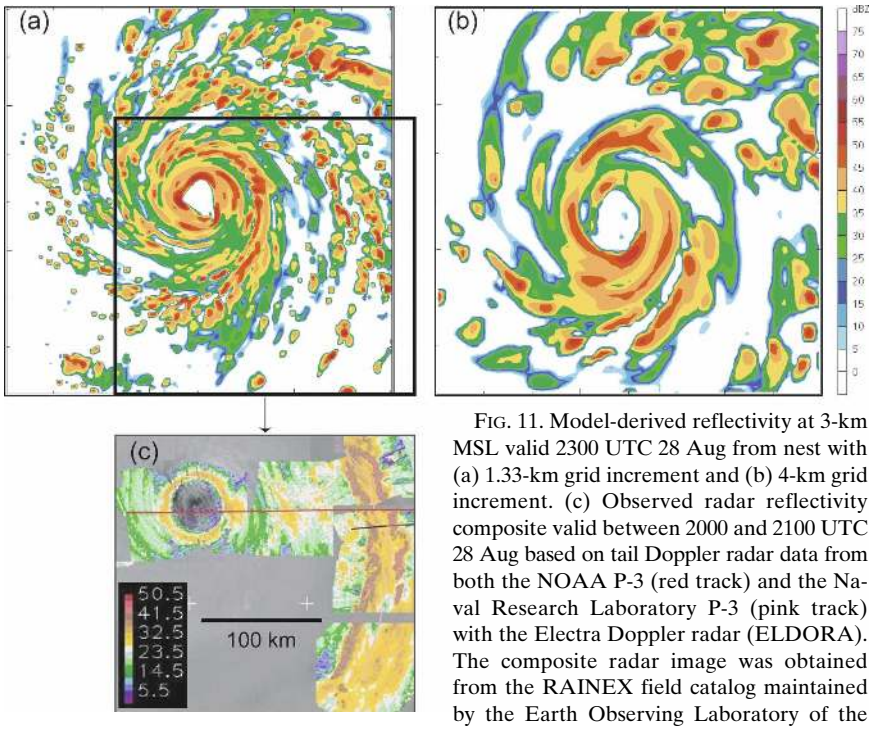

FIG. 11. Model-derived reflectivity at 3-km MSL valid 2300 UTC 28 Aug from nest with (a) 1.33-km grid increment and (b) 4-km grid increment. (c) Observed radar reflectivity composite valid between 2000 and 2100 UTC 28 Aug based on tail Doppler radar data from both the NOAA P-3 (red track) and the Naval Research Laboratory P-3 (pink track) with the Electra Doppler radar (ELDORA). The composite radar image was obtained from the RAINEX field catalog maintained by the Earth Observing Laboratory of the National Center for Atmospheric Research.

of shapes from ellipses to triangles to squares, and combinations thereof. Such structures have been documented in numerical modeling (Schubert et al. 1999; Kossin and Schubert 2001; Wang 2002) and observational studies (Kuo et al. 1999; Reasor et al. 2000; Kossin and Schubert 2004; Montgomery et al. 2006) and have been associated with Rossby waves or coherent vortices located on the edge of the eye. Evidence of mesovortices in the model reflectivity field appears in Fig. 11a as enhancements of eyewall reflectivity and abrupt changes in orientation (corners). Each of these enhancements was associated with a wind and vorticity maximum (not shown). In the simulations of Katrina using a 1.33-km grid, mesovortices appeared more prevalent than in the simulation with a 4-km grid.

Using model wind and reflectivity fields at a 10-min interval, wind and reflectivity maxima were manually tracked as they moved cyclonically around the eye. Their phase speeds were found to be remarkably consistent with the dispersion relation for linear Rossby edge waves propagating on the vorticity discontinuity in a Rankine vortex (i.e., vorticity decreases abruptly to zero with increasing radius), $C_\lambda = V_{\max}[1 - (1/n)]$, where n is the number of mesovortices or azimuthal wavenumber of the asymmetry (Lamb 1932). These waves retrogress relative to the maximum tangential wind, but for $n > 1$ they progress cyclonically relative to the ground.

While the elliptical and square-shaped eye walls in the Katrina simulation are consistent with previous observations of strong tropical cyclones (Lewis and Hawkins 1982; Muramatsu 1986), the observational literature holds no documented cases of the dominant, long-lived triangular eyewall shape noted here (Fig. 11a). Furthermore, little evidence of low wavenumber perturbations is apparent in radar observations of Katrina at the time shown in Fig. 11c, or during other transects of the center by the NOAA P-3 on 28 and 29 August (not shown). The question is whether this discrepancy has a dynamical explanation, pertaining to stability of the radial distribution of vorticity, or whether other sources of error must be considered.

To evaluate radial profiles of observed wind and vorticity (Fig. 12), 10-s data from two transects of the center of Katrina by the NOAA P-3 on the afternoon of 28 August were analyzed. An east–west transect occurred at roughly 2040 UTC, and a north–south transect was performed at about 2230 UTC, both at approximately 700 hPa. The data were transformed onto a regular radial grid of 1.3 km centered on the wind speed minimum. The vorticity (Fig. 12b) was calculated using centered differencing of the tangential wind (Fig. 12a) averaged over the four radial profiles. For analogous profiles of simulated wind and vorticity, radial profiles along the four cardinal directions were computed from hourly AHW output during the period 2000–2300 UTC, also at 700 hPa. These 16 profiles were averaged

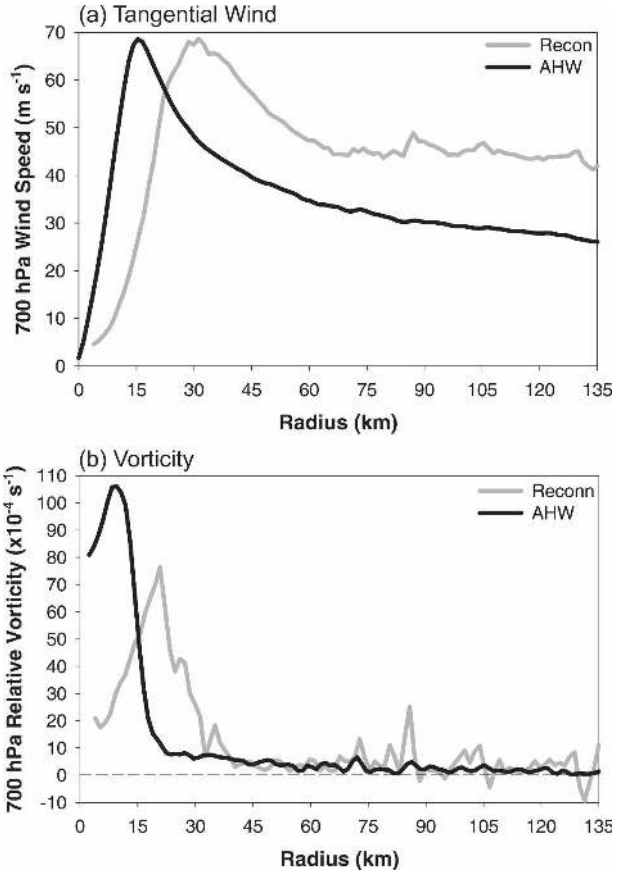

FIG. 12. Averaged radial profiles of (a) tangential wind and (b) relative vorticity from two reconnaissance transects of Katrina (2030 and 2230 UTC 28 Aug; gray) and 16 radial profiles from AHW during the period 2000–2300 UTC 28 Aug (black).

together to obtain a mean profile of tangential wind (Fig. 12a), from which vorticity was computed (Fig. 12b).

Although the maximum averaged tangential wind was similar in the simulation and observations, the simulated radius of maximum wind was about half of what was observed (Fig. 12a), and the tangential wind remained distinctly larger in the observations out to a radius of at least 135 km. In both the simulated and observed vorticity profiles, there existed a steep negative radial gradient of vorticity within and just beyond the eyewall, with a gentle vorticity gradient barely discernable farther out (Fig. 12b).

Schubert et al. (1999) showed that an important parameter in determining the most unstable wavenumber of a ring of enhanced vorticity (analogous to a hurricane eyewall) is the ratio of the inner radius of the ring to the outer radius (δ), with higher wavenumber instabilities being preferred at larger ratios. The relevant radii and their ratio are well defined for the "top hat"–like vorticity profiles of Schubert et al. (1999) and Nolan and Montgomery (2002). The latter study showed wavenumber 3 to be the most unstable in a category-3, hurricane-like vortex. From the observed radial profile of vorticity (Fig. 12b), δ is estimated to be approximately 0.15 (ratio of 5 to 33 km). However, the simulated vorticity profile does not fall to nearly zero inward from the maximum. Thus, the value of δ from the simulation is difficult to estimate. It is therefore uncertain whether the theoretical dominance of wavenumber 3 should apply to the simulation results. Other possible contributions to the production of erroneous asymmetries include (i) representing a small, nearly circular vortex on a Cartesian grid; (ii) aliasing of the marginally resolved convective cells, even with a grid spacing of 1.33 km; and (iii) the choice of microphysical scheme. Sensitivity experiments are currently under way exploring each of these alternate mechanisms.

7. Conclusions

In this article, the performance of the Advanced Hurricane WRF as applied to forecasts of five landfalling Atlantic tropical cyclones in 2005 has been examined. Results point to apparent improvements over operational models at time ranges of 48–72 h for both track and intensity prediction. The real-time forecasts also captured system-scale asymmetries of precipitation and gross asymmetries in winds. Some systematic deficiencies of the AHW were noted, however. Storms such as Katrina and Rita erroneously intensified just prior to landfall in the United States. The forecasts of intensity for the first 24 h were notably worse than for operational models, and rapid intensification was poorly handled in Katrina, Rita, and Wilma. The remainder of the paper described several improvements implemented in the AHW designed specifically to address these problems in a model configuration that is feasible to run either in research mode or routinely in real time.

Different surface energy flux formulations were tested based on results in Black et al. (2007) and earlier studies (Carlson and Boland 1978; Donelan et al. 2004). A formulation in which the drag coefficient was constant for wind speeds beyond about 30 m s^{-1}, together with a formulation of an enthalpy flux that approached roughly 0.7 times the value of the drag coefficient at high wind speeds, produced the most realistic results for the case of Katrina.

Coupling of the AHW to a simple mixed layer ocean model, derived from the original model proposed by Pollard et al. (1973), was investigated. For hurricane Katrina, the columnar 1D model produced SST changes of a similar magnitude to those observed for realistic (but spatially uniform) initial values of mixed layer depth and deep-layer lapse rate. While there are

clear limitations of the simple formulation, it nonetheless captures an important component of the effect of ocean mixing on SST. Initialization of the ocean thermal state is a key issue. It is suggested that reasonable results can be obtained if both the initial depth of the mixed layer and the deep-layer stratification are allowed to vary spatially. However, research is required to understand how satellite altimetry data can be combined with available ocean profiles to initialize directly the mixed layer model.

A key shortcoming of real-time forecasts was the lack of dynamic initialization. Even with the finer-resolution GFDL initial condition, significant adjustment of the vortex occurred within the first 12 h. This shortcoming strongly supports the need for a data assimilation and initialization procedure that is specific to the AHW. Advanced data assimilation methods are currently being tested for use with the AHW and results will be reported in a future article.

With the addition of a second nest with 1.33-km grid spacing, the simulation intensified Katrina more rapidly early on 28 August, in accordance with observations, and produced rainbands with structure more realistic than on a 4-km grid. However, simulated mesovortices in the eyewall achieved an amplitude too large compared with radar observations of eyewall reflectivity asymmetries.

Overall, it is found that track prediction is improved little, if at all, by the addition of high-resolution nests. Intensity prediction, as measured by maximum sustained winds, has not been systematically improved with the addition of a nest with a 4-km grid increment, either, but there are indications that further reduction of the grid increment around the storm core is beneficial. Future work will more systematically evaluate the benefits of using a grid spacing of 1–2 km covering the inner core.

Uncertainties associated with the surface-flux formulation are at least as large as those due to the variation of intensity with grid spacing. Echoing Chen et al. (2007), it is likely that substantive improvements of air–sea exchange will require fully coupled wave–ocean–atmosphere models. Uncertainties associated with other physical processes, such as cloud microphysics, have not been addressed herein. Zhu and Zhang (2006) and McFarquhar et al. (2006) highlight the possible sensitivity of inner-core structure to changes in microphysics, consistent with earlier results from axisymmetric models (Lord et al. 1984). It is apparent that a systematic evaluation of this sensitivity is warranted in future work.

While numerous realistic features of hurricanes appear in the model with convection represented explicitly, these structures have yet to be quantified objectively. The appearance of such detailed structures as models like AHW increase their resolution demands renewed efforts in verification of simulated processes on scales of a few kilometers. This will require new measures of forecast performance and comparison with the plethora of observations collected and archived each hurricane season. It will also require quantification of the degree to which features may be predicted deterministically and what model requirements (resolution in particular) are necessary to do so.

Acknowledgments. The authors acknowledge the assistance of Mike Black, Rob Rogers, and Mark Powell from the Hurricane Research Division of NOAA's Atlantic Oceanographic and Meteorological Laboratory in Miami. We also thank Morris Weisman of NCAR and three anonymous reviewers for their valuable comments on the manuscript.

REFERENCES

Bao, J.-W., S. A. Michelson, and J. M. Wilczak, 2002: Sensitivity of numerical simulations to parameterizations of roughness for surface heat fluxes at high winds over the sea. *Mon. Wea. Rev.,* **130,** 1926–1932.

Bender, M., cited 2005: A proposal for transition of research to operations: Upgrades to the operational GFDL hurricane prediction system. Joint Hurricane Testbed Final Rep. [Available online at http://www.nhc.noaa.gov/jht/2003-2005reports/GFDLbender_JHTfinalreport.pdf.]

Black, P. G., and Coauthors, 2007: Air–sea exchange in hurricanes: Synthesis of observations from the Coupled Boundary Layer Air–Sea Transfer experiment. *Bull. Amer. Meteor. Soc.,* **88,** 357–374.

Braun, S. A., and W.-K. Tao, 2000: Sensitivity of high-resolution simulations of hurricane Bob (1991) to planetary boundary layer parameterizations. *Mon. Wea. Rev.,* **128,** 3941–3961.

——, M. T. Montgomery, and X. Pu, 2006: High-resolution simulation of hurricane Bonnie (1998). Part I: The organization of eyewall vertical motion. *J. Atmos. Sci.,* **63,** 19–42.

Carlson, T. N., and F. E. Boland, 1978: Analysis of urban-rural canopy using a surface heat flux/temperature model. *J. Appl. Meteor.,* **17,** 998–1013.

Charnock, H., 1955: Wind stress on a water surface. *Quart. J. Roy. Meteor. Soc.,* **81,** 639–640.

Chen, S. S., 2006: Overview of RAINEX modeling of 2005 hurricanes. Preprints, *27th Conf. on Hurricanes and Tropical Meteorology,* Monterey, CA, Amer. Meteor. Soc., 12A.2.

——, J. F. Price, W. Zhao, M. A. Donelan, and E. J. Walsh, 2007: The CBLAST-Hurricane Program and the next-generation fully coupled atmosphere–wave–ocean models for hurricane research and prediction. *Bull. Amer. Meteor. Soc.,* **88,** 311–317.

Done, J., C. Davis, and M. Weisman, 2004: The next generation of NWP: Explicit forecasts of convection using the Weather Research and Forecast (WRF) Model. *Atmos. Sci. Lett.,* **5,** 110–117.

Donelan, M. A., B. K. Haus, N. Reul, W. J. Plant, M. Stiassnie, H. C. Graber, O. B. Brown, and E. S. Saltzman, 2004: On the limiting aerodynamic roughness of the ocean in very strong winds. *Geophys. Res. Lett.,* **31,** L18306, doi:10.1029/2004GL019460.

Elsberry, R. L., 2005: Achievement of USWRP hurricane landfall research goal. *Bull. Amer. Meteor. Soc.,* **86,** 643–645.

Emanuel, K. A., 1995: Sensitivity of tropical cyclones to surface exchange coefficients and a revised steady-state model incorporating eye dynamics. *J. Atmos. Sci.,* **52,** 3969–3976.

——, C. DesAutels, C. Holloway, and R. Korty, 2004: Environmental control of tropical cyclone intensity. *J. Atmos. Sci.,* **61,** 843–858.

Fowle, M. A., and P. J. Roebber, 2003: 2003: Short-range (0–48 h) numerical prediction of convective occurrence, mode, and location. *Wea. Forecasting,* **18,** 782–794.

Garratt, J. R., 1992: *The Atmospheric Boundary Layer.* Cambridge University Press, 316 pp.

Goerss, J. S., 2006: Prediction of tropical cyclone track forecast error for Hurricanes Katrina, Rita, and Wilma. Preprints, *27th Conf. on Hurricanes and Tropical Meteorology,* Monterey, CA, Amer. Meteor. Soc., 11A.1.

Hong, S.-Y., and H.-L. Pan, 1996: Nocturnal boundary layer vertical diffusion in a medium-range forecast model. *Mon. Wea. Rev.,* **124,** 2322–2339.

——, J. Dudhia, and S.-H. Chen, 2004: A revised approach to ice microphysics process for the bulk parameterization of clouds and precipitation. *Mon. Wea. Rev.,* **132,** 103–120.

Janjic, Z. I., 2004: The NCEP WRF core. Preprints, *16th Conf. on Numerical Weather Prediction,* Seattle, WA, Amer. Meteor. Soc., 12.7.

Koch, S. E., B. S. Ferrier, M. T. Stoelinga, E. J. Szoke, S. J. Weiss, and J. S. Kain, 2005: The use of simulated radar reflectivity fields in the diagnosis of mesoscale phenomena from high-resolution WRF model forecasts. Preprints, *11th Conf. on Mesoscale Processes,* Albuquerque, NM, Amer. Meteor. Soc., J4J.7.

Kossin, J. P., and W. H. Schubert, 2001: Mesovortices, polygonal flow patterns, and rapid pressure falls in hurricane-like vortices. *J. Atmos. Sci.,* **58,** 2196–2209.

——, and ——, 2004: Mesovortices in hurricane Isabel. *Bull. Amer. Meteor. Soc.,* **85,** 151–153.

Krishnamurti, T. N., 2005: The hurricane intensity issue. *Mon. Wea. Rev.,* **133,** 1886–1912.

Kuo, H.-C., R. T. Williams, and J.-H. Chen, 1999: A possible mechanism for the eye rotation of Typhoon Herb. *J. Atmos. Sci.,* **56,** 1659–1673.

Lamb, H., 1932: *Hydrodynamics.* Dover, 732 pp.

Large, W. G., and S. Pond, 1981: Open ocean momentum flux measurements in moderate to strong winds. *J. Phys. Oceanogr.,* **11,** 324–336.

Lewis, B. M., and H. F. Hawkins, 1982: Polygonal eye walls and rainbands in hurricanes. *Bull. Amer. Meteor. Soc.,* **63,** 1294–1300.

Liu, Y., D.-L. Zhang, and M. K. Yau, 1997: A multiscale numerical study of hurricane Andrew (1992). Part I: Explicit simulation and verification. *Mon. Wea. Rev.,* **125,** 3073–3093.

Lord, S. J., H. E. Willoughby, and J. M. Piotrwicz, 1984: Role of a parameterized ice-phase microphysics in an axisymmetric, nonhydrostatic tropical cyclone model. *J. Atmos. Sci.,* **41,** 2836–2848.

Marks, F. D., and L. K. Shay, 1998: Landfalling tropical cyclones: Forecast problems and associated research opportunities. *Bull. Amer. Meteor. Soc.,* **79,** 305–323.

McFarquhar, G. M., H. Zhang, G. Heymsfield, R. Hood, J. Dudhia, J. B. Halverson, and F. Marks Jr., 2006: Factors affecting the evolution of hurricane Erin (2001) and the distributions of hydrometeors: Role of microphysical processes. *J. Atmos. Sci.,* **63,** 127–150.

Michalakes, J., J. Dudhia, D. Gill, T. Henderson, J. Klemp, W. Skamarock, and W. Wang, 2005: The Weather Research and Forecast Model: Software architecture and performance. *Proc. 11th ECMWF Workshop on High Performance Computing in Meteorology,* G. Mozdzynski, Ed., World Scientific, 156–168. [Available online at http://wrf-model.org/wrfadmin/docs/ecmwf_2004.pdf.]

Montgomery, M. T., M. M. Bell, S. D. Abersen, and M. L. Black, 2006: Hurricane Isabel (2003): New insights into the physics of intense storms. Part I: Mean vortex structure and maximum intensity estimates. *Bull. Amer. Meteor. Soc.,* **87,** 1335–1347.

Muramatsu, T., 1986: The structure of polygonal eye of a typhoon. *J. Meteor. Soc. Japan,* **64,** 913–921.

Noh, Y., W. G. Cheon, S. Y. Hong, and S. Raasch, 2003: Improvement of the K-profile model for the planetary boundary layer based on large eddy simulation data. *Bound.-Layer Meteor.,* **107,** 421–427.

Nolan, D. S., and M. T. Montgomery, 2002: Nonhydrostatic, three-dimensional perturbations to balanced, hurricane-like vortices. Part I: Linearized formulation, stability, and evolution. *J. Atmos. Sci.,* **59,** 2989–3020.

Paulson, C. A., 1970: The Mathematical representation of wind speed and temperature profiles in the unstable atmospheric surface layer. *J. Appl. Meteor.,* **9,** 857–861.

Pollard, R. T., P. B. Rhines, and R. O. R. Y. Thompson, 1973: The deepening of the wind-mixed layer. *Geophys. Fluid Dyn.,* **3,** 381–404.

Price, J. F., 1981: Upper ocean response to a hurricane. *J. Phys. Oceanogr.,* **11,** 153–175.

Reasor, P. D., M. T. Montgomery, F. D. Marks Jr., and J. F. Gamache, 2000: Low-wave number structure and evolution of the hurricane inner core observed by airborne dual-Doppler radar. *Mon. Wea. Rev.,* **128,** 1653–1680.

Scharroo, R., W. H. F. Smith, and J. L. Lillibridge, 2005: Satellite altimetry and the intensification of hurricane Katrina. *Eos, Trans. Amer. Geophys. Union,* **86,** 366–367.

Schubert, W. H., M. T. Montgomery, R. K. Taft, T. A. Guinn, S. R. Fulton, J. P. Kossin, and J. P. Edwards, 1999: Polygonal eyewalls, asymmetric eye contraction, and potential vorticity mixing in hurricanes. *J. Atmos. Sci.,* **56,** 1197–1223.

Skamarock, W. C., J. B. Klemp, J. Dudhia, D. O. Gill, D. M. Barker, W. Wang, and J. G. Powers, 2005: A description of the Advanced Research WRF version 2. NCAR Tech. Note TN-468+STR, 88 pp.

Wang, Y., 2002: Vortex Rossby waves in a numerically simulated tropical cyclone. Part II: The role in tropical cyclone structure and intensity changes. *J. Atmos. Sci.,* **59,** 1239–1262.

Webb, E. K., 1970: Profile relationships: The log-linear range, and extension to strong stability. *Quart. J. Roy. Meteor. Soc.,* **96,** 67–90.

Wong, M. L. M., and J. C. L. Chan, 2004: Tropical cyclone intensity in vertical wind shear. *J. Atmos. Sci.,* **61,** 1859–1876.

Yau, M. K., Y. Liu, D.-L. Zhang, and Y. Chen, 2004: A multiscale numerical study of Hurricane Andrew (1992). Part VI: Small-scale inner-core structures and wind streaks. *Mon. Wea. Rev.,* **132,** 1410–1433.

Zhu, T., and D.-L. Zhang, 2006: Numerical simulation of hurricane Bonnie (1998). Part II: Sensitivity to varying cloud microphysical processes. *J. Atmos. Sci.,* **63,** 109–126.

——, ——, and F. Weng, 2004: Numerical simulation of hurricane Bonnie (1998). Part I: Eyewall evolution and intensity changes. *Mon. Wea. Rev.,* **132,** 225–241.